Iranian Journal of Catalysis 7(4), 2017, 303-315

IRANIAN JOURNAL OF CATALYSIS

Developments of modified magnetic nanoparticle -supported heteropolyacid catalytic performances in dibenzothiophene desulfurization

Hossein Salavati[a,*], Abbas Teimouri[a], Shahnaz Kazemi[b]

[a]*Department of Chemistry, Payame Noor University, 19395-3697, Tehran, Iran.*

[b]*Department of Chemistry, Birjand University, 97179-414, Birjand, Iran.*

Received 22 May 2017; received in revised form 1 July 2017; accepted 16 September 2017

ABSTRACT

In this research, Keggin-type polyoxometalate, $H_5PMoV_2O_{40}$ (denoted as PMoV) was immobilized on modified $NiFe_2O_4$ nanoparticles to produce a magnetically separable catalyst. This catalyst was characterized using X-ray diffraction (XRD), Fourier-transform infrared spectroscopy (FT-IR), field emission scanning electron microscopy (FESEM), cyclic voltummetry (CV), energy dispersive X-ray (EDX) and UV-vis diffuse reflectance spectroscopy (UV-DRS). The catalytic activity of synthesized catalyst in oxidation of dibenzothiophene (DBT) to dibenzothiophene sulfone ($DBTO_2$) was investigated using H_2O_2 as an oxidant and acetonitrile as an extractant. The catalyst could be readily separated from the catalytic system using the magnetic field; and loss of activity was negligible when the catalyst was recovered in five consecutive runs. The effects of main process variables including H_2O_2 amount (mmol), reaction temperature (°C) and reaction time (min) were analyzed by response surface methodology (RSM) based on the central composite design (CCD). The optimal condition for conversion of DBT was found to be H_2O_2 2.8 mmol, reaction temperature 42°C and reaction time 57 min for 0.1 g of catalyst dosage. The conversion of DBT to $DBTO_2$ under optimized conditions was 85.9 %. Moreover, the dibenzothiophene sulfone product was characterized by NMR, FT-IR, Mass and GC analysis.

***Keywords**: Heteropolyacid, Magnetic nanoparticles, Oxidation, Supported catalyst.*

1. Introduction

Desulfurization of model oil has become an environmentally important worldwide phenomenon [1,2]. Compared to traditional hydrodesulfurization method (HDS), oxidative desulfurization (ODS) is more efficient for desulfurization because it needs no harsh conditions such as gaseous hydrogen, high pressure and temperature [3]. Different catalysts, especially oxygenated molybdenum and tungsten compounds, have been accounted for oxidative desulfurization. Among them, the interest for the use of hetropolyacids (HPAs) has been expanded significantly due to their high activities in mild conditions for catalytic oxidation reactions [4,5]. In addition, among different structures of polyoxo metalates as the oxidation catalysts, Keggin type hetropolyacid is of particular importance because of its high chemical and mechanical resistance under reaction conditions.

*Corresponding author email: hosseinsalavati@pnu.ac.ir
Tel: +98 31 3352 1804; Fax: +98 31 3352 1802

In addition, the lowest vacant *d* molecular orbital in octahedra (MO_6) of this structure is nonbonding metal-centered causing its reversible reduction to form multivalence species [6,7]. Disregarding every one of these capacities, HPAs have low surface area and high solubility in aqueous media which limit their applications in catalytic reactions. The main obstacle to industrial applications of homogeneous polyoxo metalates is that they are difficult to recover from the reaction medium. Therefore, these materials are generally immobilized on suitable supports [8-12]. Many supports such as MCM-41, polyaniline (PANI) and bentonite have been used in our previous reports for the preparation of supported catalysts from polyoxometalate and investigation of catalytic and photocatalytic activities [13-15]. Magnetic nanoparticles (MNPs), which are available from accessible materials via the simple method of synthesis and which are easily separable by magnetic fields, have attracted much attention in the past few decades due to their vast applications including drug delivery,

biosensors, supported immobilization, environmental remediation and so on [16-18]. Recently, their application as catalyst supports has become a hot subject due to unique properties such as high surface area, good dispersion, magnetic behavior as well as low toxicity [19]. The most attractive feature of MNP-supported catalysts is that they can be recycled by simple magnetic separation, thereby eliminating the requirement of catalyst filtration and centrifugation [20-24]. Furthermore, improved activity is usually achieved in the nanometre-sized supported catalyst due to its high surface area and good dispersion properties. In the past few years, several transition-metal catalysts, enzyme catalysts and organocatalysts have been successfully immobilized on MNPs with good catalytic activity and reusability [25]. Most of these MNP-supported catalysts employed covalent and electrostatic immobilization strategies requiring additional synthetic manipulation in most cases [26]. Polyoxometalate immobilized on magnetic nanoparticles has been synthesized via various methods. Silica-coated CoFe nanoparticles, for example, were synthesized and used in the oxidative desulfurization of model oil [27]. Magnetic polyoxometalates (POMs) were prepared through some kind of simple sonication between functionalized magnetic nanoparticles and polyoxometalates by Zheng et al. [18]. A new magnetically separable catalyst consisting of phosphotungstic acid (PTA) supported on imidazole functionalized silica coated cobalt ferrite nanoparticles was also prepared under solvent-free conditions at room temperature. The mutual interactions between variables are described by the graphical representation of the equations called response surfaces. The application of statistical methods for optimizing adsorption process involves less treatment time, low costs and higher percentage yields. In the study, in which Design-expert 7.0.0 software (Stat Ease, USA) was used, central composite design (CCD) was employed with 20 experiments. Artificial neural network (ANN) was used for designing the process modeling M [28]. Formal batch adsorption studies depend on different process parameters such as initial solution pH, initial adsorbate concentration, catalyst amount, temperature, etc. However, this approach does not determine the combined effect of all process parameters. For scale-up studies, conventional batch process is time-consuming, and (which may be unreliable) requires a large number of experiments to determine the optimum levels, thereby increasing the overall cost of the process. In this work, ODS reaction was carried out in a biphasic system comprising acetonitrile as polar solvent and n-octane as non-polar phase, using H_2O_2 as an oxidant. The effects of reaction temperature, reaction time and molar ratio of O/S on the sulfur oxidation were investigated. Central composite design (CCD) procedure was used to investigate the influence of process factors on catalytic oxidative desulfurization reactions as a new method to optimize factors. The ODS mechanism was discussed and reusing tests were performed.

2. Experimental

2.1. Materials

All materials, which were of commercial reagent grade, were obtained from Merck, Aldrich and Fluka and used without further purification. X-ray diffraction (XRD) patterns were recorded with a Philips X-ray diffractometer (Model PW1840). FT-IR spectra were obtained as potassium bromide pellets in the range of 400–4000 cm^{-1} with Nicollet Impact 400 D spectrometer. Field emission scanning electron micrographs (FESEM) of the catalyst and reinforcement were taken using SEM Philips XL 30. Cyclic voltummetry (CV) were taken on Metrohm (model 797 VA) Processor instrument. Design expert version 7.0.0 (Stat Ease, USA) was applied for optimization of the process variables, and to evaluate the effects and complex interactions of each process variable. NMR spectra were recorded in $CDCl_3$ on a Bruker 250 MHz spectrometer. Gas chromatography experiments (GC) were performed on a Shimadzu GC-16A instrument using a 2 m column packed with silicon DC-200 or Carbowax 20 m utilizing n-decane as the internal standard. The mass spectra were recorded by the GSMS-QP 5050 Shimadzu. Magnetic properties of the supported catalyst were assessed with a vibrating-sample magnetometer (VSM, Homade 2 tesla). A magnet (Φ 17.5×20 mm, 5500 Oe) was used for collection of magnetic particles.

2.2. Preparation of Keggin type polyoxometalate (denoted as PMoV)

Keggin type polyoxometalate (PMoV) was synthesized by a technique reported beforehand. In this technique, 18.0 g of $Na_2HPO_4.12H_2O$ was dissolved in 250 ml distilled water and 11.5 g of V_2O_5 was dissolved in 100 ml of 2 mol /L Na_2CO_3 solution. They were then mixed and heated until boiling. After thirty minutes, a 400 ml solution containing 121.0 g of $Na_2MoO_4.2H_2O$ was added into the above solution, the temperature was kept at 90°C for 30 min. Then, 1:1 H_2SO_4 was added (dropwise and with stirring) to the solution until pH= 2. The mixture was cooled to room temperature under stirring, and 50 ml ether was added [29].

2.3. Preparation of $NiFe_2O_4$ nanoparticles (denoted as NiFe)

For synthesize of $NiFe_2O_4$ nanoparticles, a 0.4 M (20 mL) solution of iron nitrate ($Fe(NO_3)_3{\cdot}9H_2O$) and a 0.2 M (20 mL) solution of nickel nitrate ($Ni(NO_3)_2{\cdot}6H_2O$) were mixed in deionized water. A specified amount of polyvinyl propylene (PVP) was added to the solution as a surfactant and coating material. A 5 ml solution of hydrazine hydrate ($NH_2.NH_2.H_2O$) was slowly added to the above solution. The reactants were vigorously stirred using a magnetic stirrer. The liquid precipitate was then brought to a reaction temperature of 80°C and stirred for 2 h. The product was then cooled to room temperature. The precipitate was subsequently centrifuged with ethanol and deionized water three times. Finally, the product was dried in a hot air oven at 100°C for 4 h [30].

2.4. Preparation of modified NiFe nanoparticles (denoted as modified NiFe)

The modified NiFe nanoparticles were synthesized by the ultrasonic irradiation method; in this method, 0.04 g NiFe nanoparticles were dispersed in ethanol/H_2O (1:1) and placed under ultrasonic irradiation for 30 min (solution 1). After that, the solution of tetraethylorto silica (1 mL) and 20 mL water (solution 2) were added to this slurry. The mixture was stirred for 10 min, then the 5 mL of ammonia solution (25% w/w) was added slowly. This mixture was stirred for 24 h under magnetic stirring after that centrifuged, washed by water and dried in air. The obtained material was abbreviated as modified NiFe.

2.5. Preparation of supported catalyst (denoted as PMoV@ modified NiFe)

The polyoxometalate supported on the surface of modified NiFe nanocomposite was synthesized through bond formation between hydroxyl groups on the surface of modified NiFe and metal ions in Keggin type polyoxometal. The synthesis of PMoV supported on modified NiFe was carried out by dissolving PMoV (0.5 g) in ethanol (5 mL). This solution was added drop-wise to a synthesized modified NiFe (0.5 g in 20 mL ethanol) with dispersion by sonication for 1h at 25°C. The mixture was stirred to obtain PMoV @ modified NiFe magnetic nanoparticles. The catalyst was collected using a permanent magnet and dried under vacuum for 24 h at 25°C.

2.6. Catalytic activity

Since heterogeneous catalysts are recoverable, heterogenization of catalysts is of incredible interest. Therefore, we decided to immobilize PMoV on $NiFe_2O_4$ nanoparticles, and investigate its catalytic activity in the oxidation of dibenzothiophene (denoted as DBT) with H_2O_2 under magnetic stirring.

3. Results and Discussion

3.1. Catalyst characterization

The FT-IR spectra of $NiFe_2O_4$, PMoV, modified NiFe and PMoV@ modified NiFe are shown in Fig. 1. All samples showed two intense and broad peaks at around 3448 and 1622 cm^{-1}, which were associated with the stretching vibrations of free or adsorbed water remaining in the sample. Two mainboard metal-oxygen bands were found in the IR spectrum of NiFe spinel and ferrites in particular. The highest one, $\bar{\nu}_1$, (Fig. 1a) is for the most visible part in the range of 500-600 cm^{-1}, corresponding to intrinsic stretching vibrations of the metal at the tetrahedral site, $M_{tetra} \rightarrow O$, whereas the $\bar{\nu}_2$, lowest band, which is generally watched in the range of 385-450 cm^{-1}, is given to octahedral metal stretching vibration, $M_{octa} \rightarrow O$ [30]. It is known that Ni^{2+} ions have octahedral-site preference. Fe^{2+} and Fe^{3+} ions can occupy both octahedral and tetrahedral sites. The bands at 1087 cm^{-1} along with the shoulder at 1200 cm^{-1} correspond to the stretching mode of the Si–O–Si bond in silica, and the band at 464 cm^{-1} is assigned to Si–O–Si or O–Si–O bending modes (Fig. 1b). FT-IR spectrum of the Keggin type polyoxometalate (PMoV) showed absorption bands at 1059 cm^{-1}, 961 cm^{-1}, 842 cm^{-1} and 775 cm^{-1} corresponding to the four typical skeletal vibrations of the Keggin type polyoxoanions (Fig. 1c). FT-IR spectrum of the prepared catalyst showed absorption bands at 1054 cm^{-1}, 955 cm^{-1}, 846 cm^{-1} and 775 cm^{-1} corresponding to the four typical skeletal vibrations of the Keggin type polyoxoanions (Fig. 1d) [29] with the shift due to the immobilization of Keggin type polyoxometalate on the surface of modified NiFe magnetic nanoparticles. This indicated that PMoV was supported on modified NiFe. These peaks could be attributed to, $\bar{\nu}$ (P=Oa), $\bar{\nu}$ (Mo=Ot), $\bar{\nu}$ (Mo-O_b-Mo) and $\bar{\nu}$ (Mo-O_c-Mo), respectively (Ot= terminal oxygen, O_b= bridged oxygen of two octahedral sharing a corner and O_c= bridged oxygen sharing an edge). The presence of Ni–O and Fe–O bonds in $NiFe_2O_4$ was confirmed by the peaks at 416 cm^{-1} and 594 cm^{-1} which were shifted to 464 cm^{-1}, 596 cm^{-1} after coating with silica. In addition, the peak related to OH groups in adsorbed water shifted to lower peak, which could be due to the immobilization of Keggin type polyoxometalate on the modified NiFe nanoparticles, and confirmed that the Keggin type polyoxometalate was successfully immobilized on the modified NiFe.

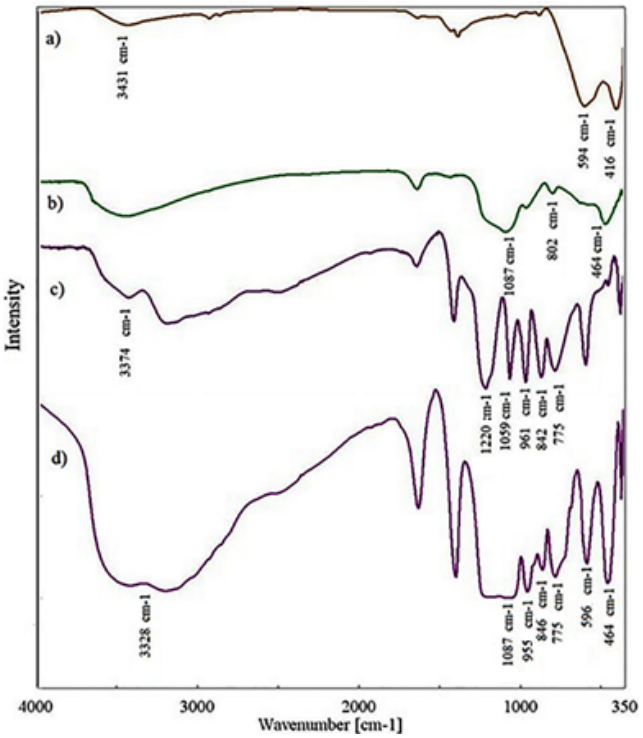

Fig. 1. FT-IR spectra of a) NiFe b) modified NiFe, c) PMoV, d) PMoV@ modified NiFe.

The electronic properties of PMoV@ modified NiFe was studied using DR UV-vis spectroscopy. The DR UV-vis spectrum of PMoV showed absorption bands at 250 and 306 nm [29], which are associated with octahedrally coordinated Mo^{6+} and arise due to the Mo–O and V–O charge-transfer absorptions in the skeleton of Keggin type polyoxometalate. These two absorption bands appeared in the DRS spectrum of the prepared catalyst with shift due to immobilization of PMoV on the surface of modified NiFe, and in supported catalyst, the peaks in 245 nm and 303 nm could be related to structure of Keggin type polyoxometal (Fig. 2).

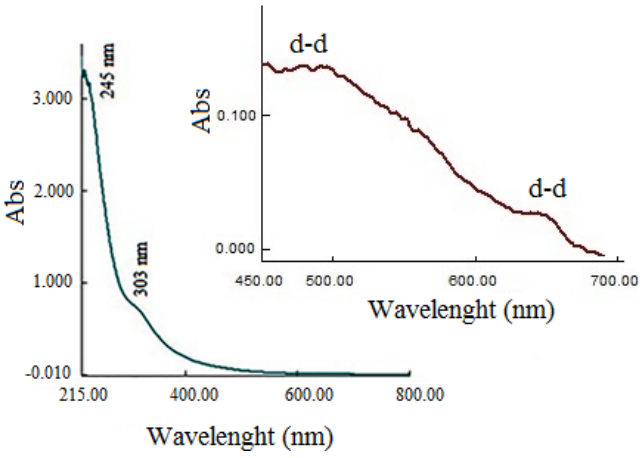

Fig. 2. DR UV-Vis spectrum of supported catalyst.

Therefore, these results indicated that primary structure of Keggin type POM has been immobilized on the surface of modified magnetic nanoparticles and showed strong interaction with catalysts. In addition the visible region with high resolution was observed and confirmed d-d transition in metal for spinel structure.

Fig. 3 shows XRD patterns of NiFe, modified NiFe and PMoV @ modified NiFe. These patterns indicated that PMoV was immobilized on the surface position of modified NiFe. In addition, characteristic peaks of PMoV in the supported catalyst confirmed that PMoV was deposited on the surface of the supported catalyst. The pattern in Fig. 3a shows that the $NiFe_2O_4$ phase crystallinity and structure of the $NiFe_2O_4$ nanocrystals were also confirmed by powder XRD. The XRD pattern of the $NiFe_2O_4$ in Fig. 3a agrees well with the powder diffraction file of JCPDS file No. 10-0325. The space group of the $NiFe_2O_4$ is Fd3m and it has an inverse spinel structure. All the characteristic peaks for $NiFe_2O_4$ were observed at 30.47° (220), 35.81° (311), 37.47° (222), 43.42° (400), 53.87° (422), 57.37° (511), 63.06° (440), 74.57° (533) [30].

After modification of NiFe nanoparticles, there are no peaks from crystalline SiO_2 because it remains amorphous due to employing the low-temperature synthetic method (Fig. 3b). When PMoV is immobilized on the surfaces of the modified NiFe magnetic particles, the characteristic peaks for PMoV are observed in modified NiFe@PMoV, which implies retention of the crystalline character of PMoV (Fig. 3c). The average particle size of PMoV@ modified NiFe powder was calculated from XRD line broadening using the Debye–Scherer equation, D= (0.89λ)/(β ½ cosθ), where k is the wavelength of Cu λa radiation, β1/2 is the full width at half maximum (FWHM) and θ is the Bragg angle.

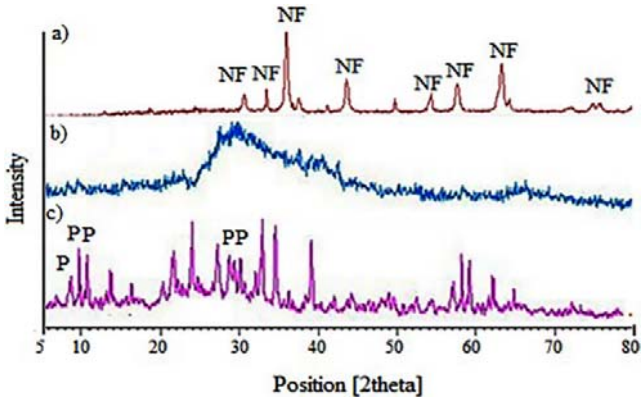

Fig. 3. XRD patterns of a) NiFe, b) modified NiFe, c) PMoV@ modified NiFe, NiFe represented by NF and polyoxometal represented by P.

The average particle size was calculated to be about 67.5 nm, which was in accordance with the FESEM and observations. The powder XRD patterns ($10<\theta<70$) obtained from the supported catalyst are shown in Fig. 3c. The peaks related to polyoxometalate skeleton were observed at $2\theta = 28.2$ and 28.9 and below $2\theta=10$ at $2\theta=8.2$, 8.9, 9.2 and 9.2 [29]. This result showed that the Keggin type polyoxometalate was successfully immobilized on the surface of modified NiFe nanoparticles.

The morphologies of NiFe, modified NiFe and PMoV@ modified NiFe, supported catalyst, were examined using FESEM. Fig. 4a shows the morphology of NiFe nanoparticles. The particle sizes of NiFe nanoparticles were estimated to be in 19-23 nm range. After the immobilization of Keggin type polyoxometalate on the modified surface of magnetic nanoparticles, clear changes in the morphology of magnetic nanoparticles and particles sizes in FESEM were observed. These results showed the immobilization of Keggin type polyoxometalate on the surface of magnetic nanoparticles. Fig. 4b shows that the FESEM image of modified NiFe and the particle size of modified NiFe nanoparticles were estimated to be in 20-25 nm range. The obtained particles were agglomerated as a consequence of strong magnetization and highest particle surface energy, using the supported catalyst. The morphologies and nanostructures of the nanoparticles were approximately spherical. Some nanoparticles were aggregated. By assuming that a nanoparticle is spherical, the average diameter of nanoparticles were estimated to be 68.4 nm which was measured in several directions in the FESEM images. The larger size could be due to the aggregation of particles (Fig. 4c).

Energy dispersive X-ray image of NiFe, modified NiFe and the supported catalyst are shown in Fig. 5. EDX image of NiFe nanoparticles showed Ni, Fe and O elements in Fig. 5a. EDX image of modified NiFe nanoparticles showed Ni, Fe, O and Si elements in Fig. 5b. For the supported catalyst, Mo, Si, V, Ni, Fe and O elements are presented in the EDX image of synthesized catalyst. The analysis revealed the excellent uniform distribution of PMoV on modified NiFe structure.

Polyoxometalates can be immobilized on electrode surfaces by various methods such as modification, immobilization as a dopant in conductive polymeric matrices, adsorption, layer-by-layer approaches and immobilization in inorganic matrices. Among these approaches, entrapment of polyoxometalate into inorganic matrix was considered as an attractive methodology for sensor fabrication due to stability and simplicity. To investigate the electrochemical behavior of PMoV supported on modified NiFe, which is insoluble in water, a three dimensional bulk modified carbon paste electrode (CPE) employing the supported catalyst was fabricated. The electrode was prepared by mixing the graphite powder as the conductive material, silicon oil as the pasting liquidand also PMoV and supported PMoV as the electro active species. The electrochemical studies were carried out in 0.2 M HCl aqueous solution, because PMoV is unstable in neutral and basic aqueous solutions. Fig. 5 shows the cyclic voltammograms in 0.2 M HCl aqueous solution at a bare CPE, and CPE modified with PMoV – modified NiFe. It can be seen from Fig. 6 that in the potential range of -1 to 2 V (vs. Ag/AgCl) there is no redox peak at the bare CPE, while some consecutive redox processes are observed at the modified CPE. The above experimental results showed that PMoV can be supported on the surface of modified NiFe. According to Fig. 6, curves a and b represent the CVs of polyoxometalate and supported catalyst respectively.

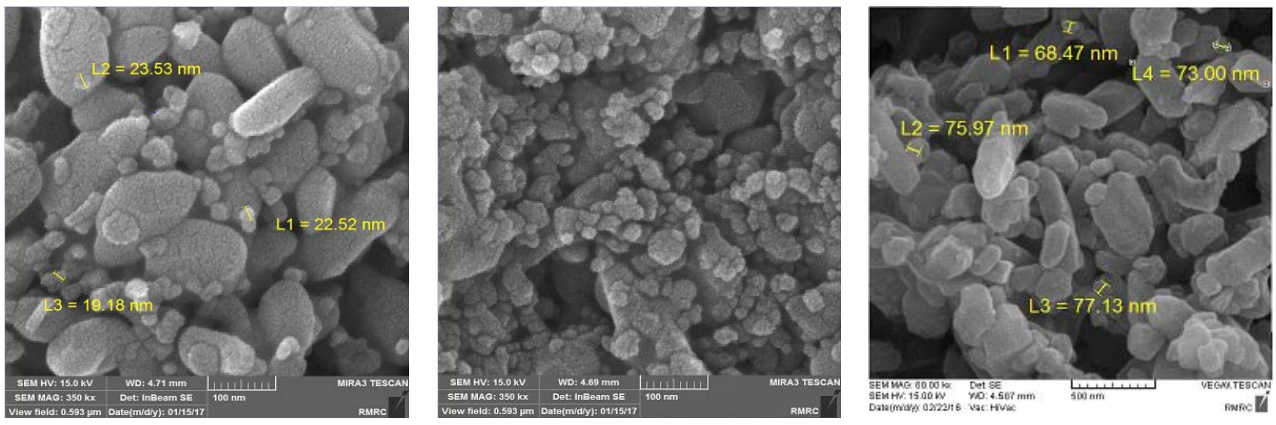

(a) **(b)** **(c)**

Fig. 4. FESEM images of a) NiFe, b) modified NiFe, c) PMoV @ modified NiFe.

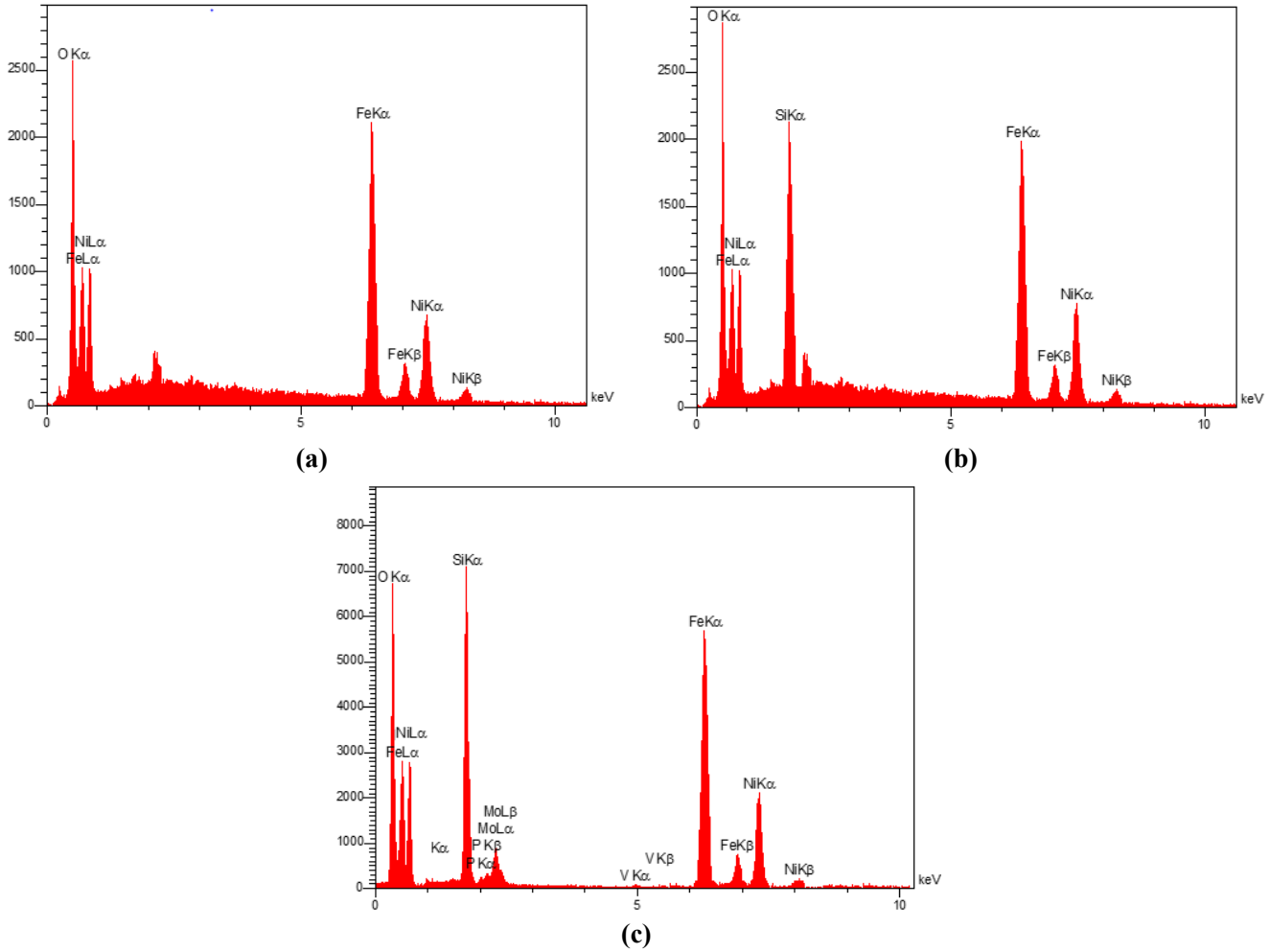

Fig. 5. EDX images of a) NiFe, b) modified NiFe, c) modified NiFe@PMoV.

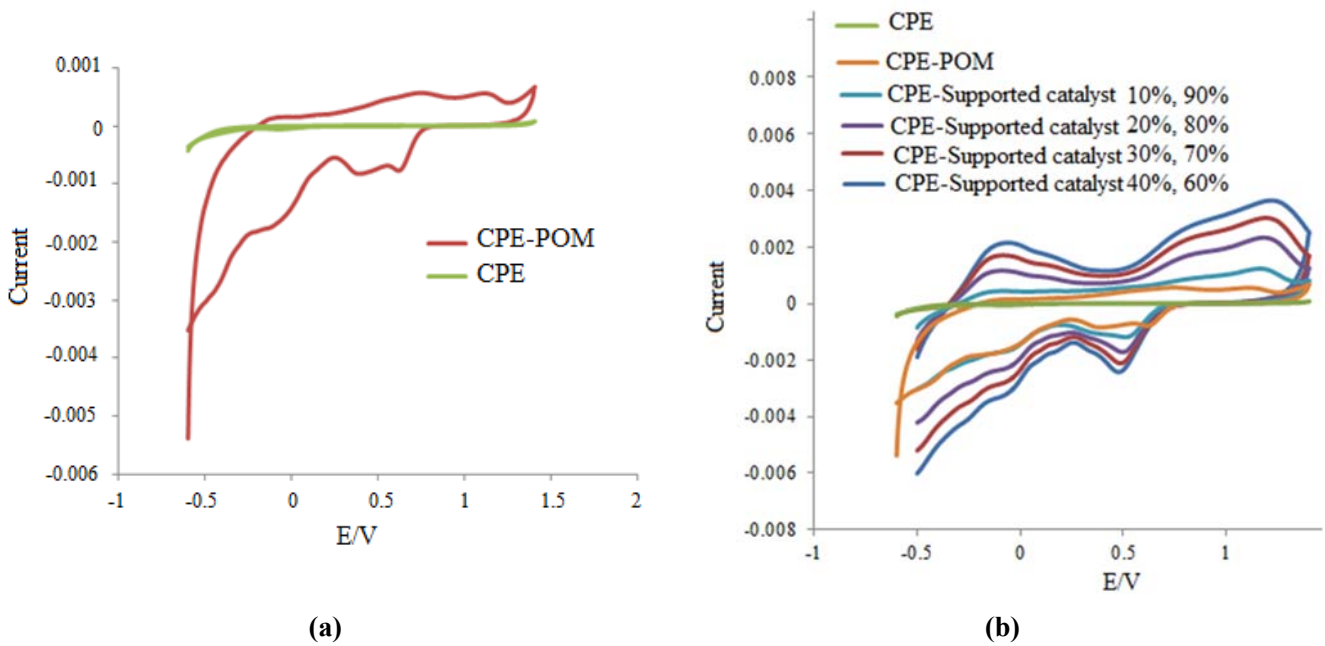

Fig. 6. Cyclic voltammograms of a) PMoV-CPE, b) PMoV@modified NiFe-CPE (x% PMoV, y% modified NiFe). The concentration of each species is 1.0 × 10-3 M.

It should be noted that electron-transfer rate of supported catalyst should be faster than polyoxometalate. The above results reveal that PMoV –modified NiFe exhibit significantly improved electrochemical performance in comparison to PMoV. The relatively good capacitive performance of the PMoV-modified NiFe has some reasons: (1) the presence of the hydroxyl groups can possess a high concentration of surface functional groups for linkage of polyoxometalate, which can enhance the electro active surface area for double-layer charge storage; (2) good dispersion of PMoV on the surface of modified NiFe would increase the accessibility of the available active sites in the supported catalyst. In addition, with increasing percentage of polyoxometalate for immobilization on the surface of modified NiFe, current in cyclic voltummetry was increased; this suggests that polyoxometalate has an important role in electron transfer and in the supported catalyst, polyoxometalate accelerates the electron transfer compared to intact polyoxometalate.

The magnetic properties of the supported catalyst were studied using a VSM. As shown in Fig. 7, the PMoV@modified NiFe catalyst was ferromagnetic. The *M*s Value was lower than that reported for bulk samples. This decrease in the *M*s could be mainly attributed to the small particle surface effect, which became more dominant as the particle size was decreased. It could arise from the greater disorder of surface spins and the presence of SiO_2 (which formed diamagnetic matrix, diluting the magnetization of the otherwise compacted ferrite particles).

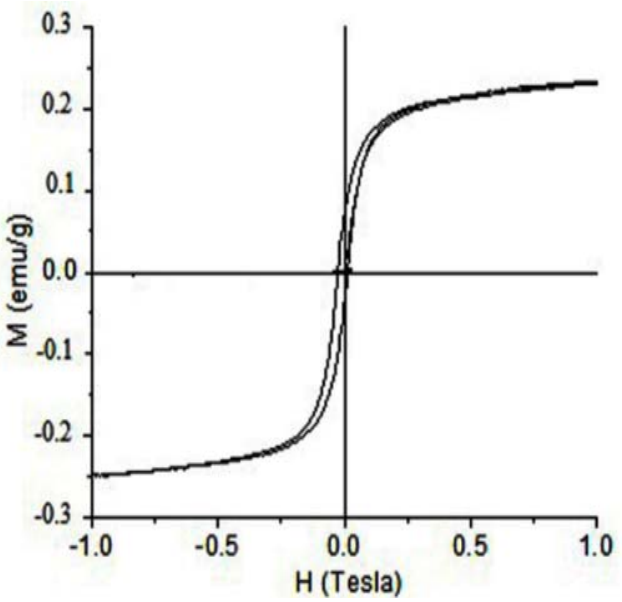

Fig. 7. Magnetic hysteresis loops for PMoV@ modified NiFe.

3.2. Oxidation reactions with hydrogen peroxide

The reactions were typically performed using H_2O_2 at 42°C in a stirred solution of the substrate (sub), catalyst (cat) and 30% (w/w) aqueous hydrogen peroxide (ox) in n-octane/ acetonitrile. The oxidation of dibenzothiophene was carried out in various conditions and the optimized conditions were obtained. The amounts of the several components used in the reactions were dependent on the substrate and are presented in the results and discussion section. The conversion and percentages of each compound in the reaction mixtures were analyzed using gas chromatography. The dibenzothiophene was selected as a model substrate. The total sulfur content of the samples was determined by microcoulometry (detection limit: 0.1 ng mL^{-1}). The compounds containing sulfur present in diesel were analyzed using a gas chromatograph coupled to a flame photometric detector (GCFPD). Gas chromatography conditions used in this work are Agilent 6890 N equipped with a capillary column (PONA, 50 m ¥ 0.2 mm, id ¥ 0.5 mm) and flame photometric detector (FPD): Agilent H9261. The analysis conditions were as follows: injection port temperature: 280°C, detector temperature: 250°C, oven temperature program: 100°C (hold for 1 min), 100–150°C at a 10°C min-1 gradient (hold for 1 min), 150–280°C at a 5°C min^{-1} gradient (hold for 12 min), split ratio: 1/100, carrier gas: ultra-pure nitrogen, column flow: 0.9 $mLmin^{-1}$, reagent gases air flow: 100 mLmin-1, hydrogen flow: 75 mL min^{-1}, the injection volume of the sample was 1 mL.

3.3. Statistical analysis and the model fitting

The influence of various factors on the catalytic oxidation of DBT was investigated and we examined effects of temperature, oxidant amount and time on the catalytic oxidation of DBT selected as a model sulfur compound for optimization. The design expert 7.0.0 software was used for regression analysis of the data and for estimation of the coefficient of the regression equation. The equations were validated by the statistical tests called ANOVA to determine the significance of each term in the fitted equations and to estimate the goodness of fit of each case. Response surfaces were drawn for the experimental results, obtained from the effect of different variables on the percentage oxidation of DBT, in order to determine the individual and cumulative effects of these variables and the mutual interactions between them. The Fisher's F value with a low probability ($p < 0.0001$) showed that the model was significant. The multiple correlation coefficient (R^2) demonstrated the suitability of the model. Moreover, R^2 value is 0.975 which could be

explained by the developed quadratic model, and the predicted R^2 values were in agreement with adjusted R^2, which means all the terms depicted in the model were significant. In this case, the non-significant lack-of-fit (0.6) confirmed that the quadratic model was valid for this process. For this research, the effectiveness of three essential operating parameters including reaction temperature (A), reaction time (B) and H_2O_2 amount (C) was systematically evaluated using the central composite design procedure. The selected variables are summarized in Table 1.

3.4. Comparison between theoretical and experimental data

The CCD equation of actual factors was solved by partial differential calculus to obtain the optimum value of A, B, C. For this research, the effectiveness of three parameters including reaction temperature (A), reaction time (B), H_2O_2 mmol (C) was systematically optimized using central composite design software. In this technique, the total number of experimental runs can be calculated by Eq. (1):

$$N=2^n+2n+ n_c \quad (1)$$

Where, n and n_c represented the variable number and the replicated number of the central point, respectively. For statistical analyses and optimization of each cycle, a quadratic model was selected as the best model and fitted to the results subjected to Eq. (2):

$$Y_m = \beta_0 + \sum_{i=1}^{n} \beta_i x_i + \sum_{i=1}^{n} \beta_{ii} x_i^2 \sum_{1\le i\le j}^{n} \beta_{ij} x_i x_j + \varepsilon \quad (2)$$

Where, Y_m is the predicated response, n is the number of variables, x_i and x_j are coded variable and β_0, β_i, β_{ii}, β_{ij} and ε are constant term, liner, square, effects of interaction between variables and the residual value, respectively. The design expert (DX7) software was applied for statistical calculations to optimize the process and determine the response model. The optimized values for theoretical and experimental study is shown below:

Theoretical: Temp.= 50.6°C, Time= 47.5 min, Oxidant= 2.8 mmol, catalyst amount= 100 mg, R (% degradation)= 89.8%.

Experimental: Temp.= 42.3°C, Time= 57 min, Oxidant= 2.8 mmol, catalyst amount= 100 mg, R (% degradation)= 85.9%

Based on the obtained conversion and optimized condition, the experimental results of CCD are listed in Table 2. This results show the significant influence of the selected operating variables, their actual values and the corresponding response (predicted values).

The experimental results of CCD showed the significant influence of the selected operating variables. The effect of three process factors including the reaction temperature (A), reaction time (B) and amount of H_2O_2 (C), and also interaction between these variables were analyzed by means of RSM methodology to obtain an empirical model for the best response. The final quadratic equation was attained to illustrate the relationship between the independent variables and the dependent responses which is displayed in Eq. (3):

$$Y_m = +99.18 + 5.27\,A + 6.50\,B + 7.52\,C - 4.40\,AB - 5.45\,AC - 2.65\,BC - 3.53A^2 - 6.64\,B^2 - 8.31C^2 \quad (3)$$

The importance degree of the tested factors based on the coefficient in the above equations on conversion was H_2O_2 amount > time > temperature. The regression plot of the trained network is shown in Fig. 8. The trained network gave a correlation coefficient of 0.975. A high correlation coefficient of this plot signified the reliability of the neural model based on the experimental data.

Statistics results of the model summary showed that the predicted R-squared= 0.868 is close to the adjusted R-squared= 0.947.

Table 1. The range of the independent variables applied in the central composite design.

Factor	Name	Units	Type	-Level	+Level	-α	+α
A	temp	centigrade	Numeric	40	70	29.7731	80.2269
B	time	min	Numeric	30	90	9.54622	110.454
C	oxidant	mmol	Numeric	2	4	1.31821	4.68179

Table 2. CCD experiment design and response result for oxidative desulfurization of DBT.

std	Runs	Temp. (°C)	Time (min)	H_2O_2 (mmol)	Experimental R%
12	1	55	110	3	94.1
14	2	55	60	4.6	89.6
1	3	40	30	2	55
17	4	55	60	3	99.2
6	5	70	30	4	89
8	6	70	90	4	82
9	7	29	60	3	78.9
3	8	40	90	2	76.2
19	9	55	60	3	99.2
5	10	40	30	4	78.2
11	11	55	9	3	65.8
2	12	70	30	2	81.2
10	13	80	60	3	98.6
18	14	55	60	3	99.2
13	15	55	60	1.3	60.9
4	16	70	90	2	91.2
20	17	55	60	3	99.2
16	18	55	60	3	99.2
7	19	40	90	4	95.2
15	20	55	60	3	99.2

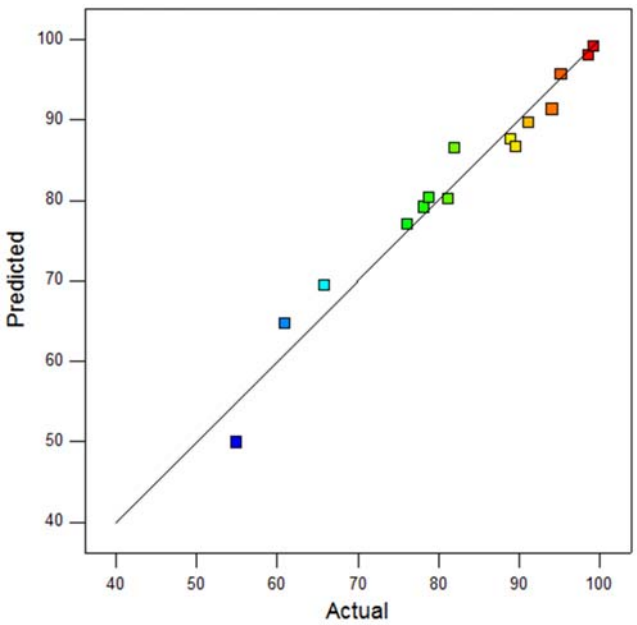

Fig. 8. Regression plot (experimentally vs. predicted) using three input variables.

This confirmed that the model is acceptable. In addition, adequate precision is a measure of the range in the anticipated response relative to its related errors. A ratio larger than four is favorable. The high ratio of 88.023 indicated an adequate ratio and this model can be utilized to navigate the design space. The small values of coefficient of variation (C. V. %) of 0.89 and standard deviation (Std. Dev.) of 0.61 indicated reliability. The small predicted residual sum of squares (PRESS) of 26.99 is a criterion of how good the model fits each point in the model. The smaller the PRESS statistic, the better the model fits the data points. The above results indicated that the proposed quadratic model guarantees an precise demonstration of the experimental data and also showed high validity and adequacy of the model in predicting the conversion percentage of DBT.

The effect of different levels of oxidant and time on oxidation of DBT using the Keggin type polyoxometalate supported on modified NiFe can be predicted from the contour plot as shown in Fig. 8.

The contour plot shows that oxidation percentage increased when oxidant amount and time enhanced. This could be due to the increase in the exposed surface area of the catalyst. However, it must be noted that after a certain limit, if the amount of oxidant had been increased further, there would have been a saturation point in which the conversion was decreased because the oxidant probably decomposed. It was observed that a maximum removal efficiency of 89.86% was achieved at 2.8 mmol oxidant, and 57 min of time. The combined effect of temperature and time on oxidation of DBT was shown in the contour plot of Fig. 8. The percentage of oxidation was enhanced with increased time due to an increase in number of molecules of sulfur compounds which were converted to sulfone. Higher temperature enhanced the catalytic active sites force and increased the oxidation of sulfur compounds. From the results it was observed that a maximum removal efficiency of 89.86% was achieved at 42°C, and in 57 min. The combined effect of temperature and oxidant amount on oxidation of DBT was observed in the contour plot of Fig. 9. It was shown that conversion increased with increasing oxidant and temperature. The maximum conversion of 89.86% was obtained from 2.8 mmol oxidant and the temperature of 42°C. As can be seen in Fig. 8 (a-f), the importance degree of the tested factors on conversion was: H_2O_2 amount > time > temperature.

It should be noted that when the catalyst was replaced by NiFe as a catalyst, no oxidation product was observed with longer reaction times up to 2 h (Fig. 1S).

3.5. Analysis of oxidation product

After the completion of the reaction, the catalyst was separated from the reaction solution using an external magnet. It should be noted that the sulfur-containing materials in oil are polar in nature because of the electronegativity sulfur atoms. Oxidation of organosulfur compounds changes their polarity to sulfoxides (DBTO) and sulfone ($DBTO_2$). They can then be easily extracted into solvent phase; the extraction-oxidation process consists of three phases: the oil phase, an extraction solvent and a solid catalyst.

When these three phases are present in the reaction media, the DBT in oil phase is extracted into solvent and the oxidant reagent produces the corresponding sulfoxide and sulfone products in an oxidation reaction. In this investigation, acetonitrile was chosen as extractant solvent. In GC analysis, the oil phase demonstrated that during oxidative process the dibenzothiophene reduced while the peaks attributed to sulfoxide and sulfone were at trace levels since time increased. By acetonitrile evaporation at room temperature, solid products were observed on the wall of vessel. Mass analysis (Fig. 2S) which recorded M^+ at *m*/*z* 216 confirmed that the sulfone of dibenzothiophene was found. The intense *m*/*z* peaks of the mentioned crystals at 187, 168 and 160 could be ascribed to $C_{11}H_7SO$, $C_{12}H_8O$ and $C_{10}H_8S$ ions moieties of dibenzothiophene S and S- dioxide, respectively [48]. An examination between FT-IR spectra of the formed crystal and dibenzothiophene is shown in Fig. 3S. Both compounds indicated almost similar bands except that in the spectrum of the mentioned crystal, two new bands with strong intensity appeared at 1286 and 1161 cm^{-1}, which could be given to the asymmetrical and symmetrical stretching vibration modes of O ← S → O, respectively [48]. Therefore, under applied experimental conditions, the dibenzothiophene compound was oxidized selectively to corresponding sulfone, and was removed from the mixture by adsorption on the surface of the synthesized catalyst. In ^{1}HNMR of dibenzothiophene, the peaks in range of 7-8 ppm determined aromatic hydrogens of phenyl ring (Fig. 4S). The conversion and percentages of each compound in the reaction mixtures were analyzed using gas chromatography (Fig. 5S).

To establish the applicability of the process, various sulfur compounds were subjected to the oxidation system using the synthesized catalyst (Table 3). The reactivity of the sulfur compounds were influenced by two main factors, i.e., the electron density on the sulfur atom band and the steric hindrance of the sulfur compound. Compared to BT, DBT shows higher reactivity, which can be explained by the higher electron density on sulfur atom of DBT. For DBT and 4,6-DMDBT, the difference in the electron density on the sulfur is very small. Therefore, the lower reactivity of 4,6-DMDBT is due to the steric hindrance of the methyl groups that limit the accessibility of the sulfur atoms to the catalytic active sites.

To investigate the effect of oxidant nature on the conversion of DBT, a series of experiments with various oxidants was applied in the oxidation reaction. The results shown in Fig. 6S indicate that the conversion of DBT in the presence of different oxidants changed from 16% to 85.5%. Sufficient catalytic sites were available to drive the reaction to completion in the presence of H_2O_2 as oxidant, and was chosen for further experiments. The highest conversion of DBT in the presence of H_2O_2 could be due to higher yield of superoxo in the oxidation reaction. In addition, blank reactions, with H_2O_2 but without catalyst and with catalyst but without H_2O_2, were performed in all conditions. Conversion values attained in the blank reaction were in the range of 5 – 32.5%.

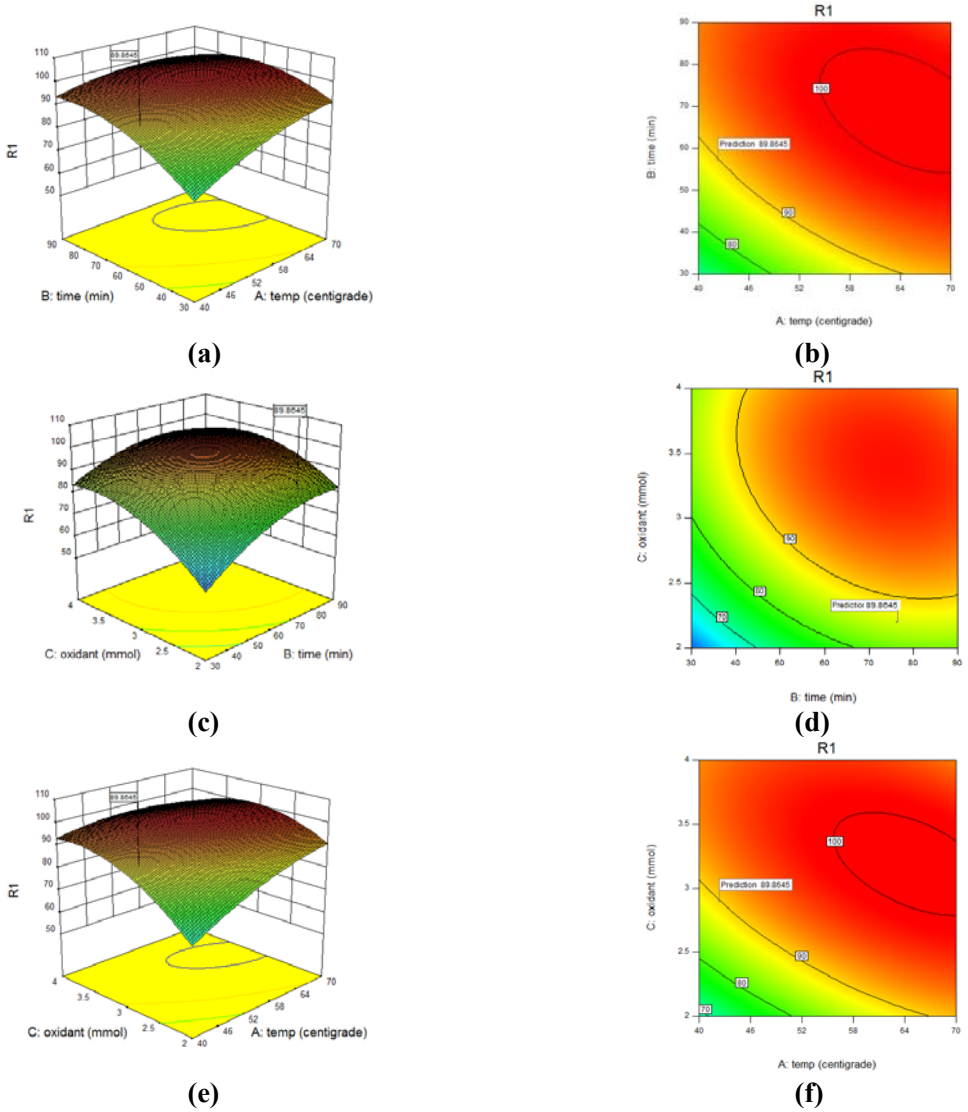

Fig. 9. Three dimensional response surface graph and counter plots for the oxidation of DBT, % dye degradation versus time and temperature, counter plots for time and temperature, % oxidation versus time and oxidant, counter plots for time and oxidant, % oxidation versus temp and oxidant, counter plots for time and oxidant, respectively with 100 mg catalyst.

Table 3. Oxidation of sulfur compound to sulfone product with H_2O_2 catalyzed by synthesized catalyst.[a]

Entry	Sulfur compounds	Structure	Yield (%)[b]
1	DBT	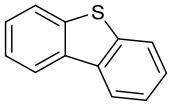	85.9
2	BT	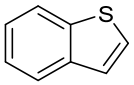	75.2
3	4,6-DMDBT	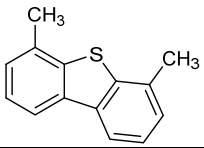	80.2

[a]Reaction conditions: Temperature (42 °C), time (57 min), H_2O_2 amount (2.8 mmol), 100 mg catalyst.
[b]GC yields based on the toluene as the internal standard.

3.6. Consideration of acid catalyst properties of synthesized catalyst

The density and strength of acid sites and the rate of catalytic reactions on metal salts catalysts were increased with the slight oxidation of the M centers, which often occurs during catalytic reactions in oxidation media environments. In addition, the more effective dispersion of metal salt species on high surface area supports the introduction of a heteroatom in order to create a permanent charge imbalance in the metal oxide structure, thereby increasing the density and strength of the acid sites. According to the definitions offered by Bronsted and Lewis acidity, a solid acid shows a tendency to donate a proton or accept an electron pair, respectively. A solid acid can also be defined as a solid on which the color of a basic indicator changes, or as a solid on which a base is chemically adsorbed [19-22]. Thus, the acidic properties of the catalysts should be considered. The proposed mechanism for acid catalyst properties of supported catalyst is shown below; immobilized ion metal in polyoxometalate reacted with H_2O_2 to generate peroxo species. This species facilitated the transfer of the electrophilic oxygen to the sulfur, yielding the corresponding epoxide. The epoxide product could be easily removed by extraction. Many investigators have suggested various mechanisms for oxidation of sulfur compounds. Scheme 1 suggests the catalytic oxidation pathways.

3.7. Catalytic behavior, separation, and recyclability

The stability of the supported catalyst was monitored using multiple sequential oxidation of DBT with synthesized catalyst under optimized conditions. For each of the repeated reactions, the catalyst was recovered, washed thoroughly with water to remove the H_2O_2 and dried before being used with fresh DBT solution. The data showed that the catalysts were recovered for five runs without the loss of activity. The yields were 85.9, 85.6, 85.3, 84.2 and 84%, respectively.

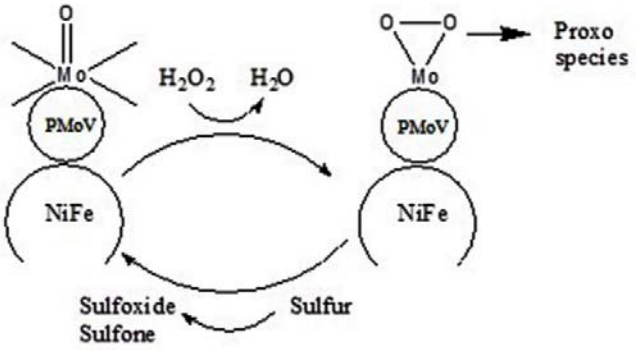

Scheme 1. Proposed mechanism for oxidation of DBT by supported catalyst.

The assessment of the stability of catalyst was performed as follows: FT-IR spectrum of the catalyst was taken and the results showed the peaks corresponding to synthesized catalyst stucture were shown at 772 cm^{-1}, (840 cm^{-1}, 950 cm^{-1}), 1081 cm^{-1}, (1200 cm^{-1} and 3319 cm^{-1}) relating to M=O, O-M-O, Si-O and O-H groups, respectively with shift due to the adsorption procedure (Fig. 7S).

Table 4 compares the catalytic activity of the supported catalyst with those of other reported catalysts for oxidation of sulfur compounds.

4. Conclusions

PMoV@ modified NiFe were prepared by anchoring PMoV on the surface of modified $NiFe_2O_4$ magnetic nanoparticles. The catalyst showed excellent catalytic activity in oxidation of DBT selected as a model sulfur compound. This catalyst could be easily separated at the end of the reaction using the magnetic field. Therefore, it could be reused at least five times, with only a slight decrease in catalytic activity. Electrochemical characterization showed that electron-transfer rate of the supported catalyst should be faster than polyoxometalate. The results showed that supported catalyst could accelerate electron transfer in catalytic procedures due to good dispersion of PMoV on the surface of modified NiFe nanoparticles.

Table 4. Comparison of reaction data for the present method in oxidation of sulfur compound and other reported methods.

Catalyst	Reaction condition	Conversion%	Ref.
PMoV@ modified NiFe	H_2O_2/42°C/57 (min)	85.9%	This work
$(Bu_4N)_4H[PMo_{10}V_2O_{40}]$–$TiO_2$	H_2O_2/80°C/120 (min)	98%	[31]
(n-$(Bu_4N)_3[PMo_{12}O_{40}]$	H_2O_2/70°C/180 (min)	40%	[32]
$(Bu_4N)[PMo_{12}O_{40}]$/UHP	4°C/72 h	85%	[33]
Silica-Based Ammonium Tungstate/H_2O_2 (30%)	CH_2Cl_2/MeOH, r.t., 1.5 h	82%	[34]

Acknowledgements

The authors are thankful to Payame Noor University in Isfahan Research Council and contributions from Brijand University are gratefully acknowledged.

References

[1] I. Frenanez, N. Khiar, Chem. Rev. 103 (2003) 3651-3701.
[2] Z. Jiang, H. Lü, Y. Zhang, Chin. J. Catal. 32 (2011) 707-715.
[3] D. Xie, Q. He, Y. Su, T. Wang, R. Xu, B. Hu, Chin. J. Catal. 36 (2015) 1205-1213.
[4] F. Yu, R. Wang, Molecules 18 (2013) 13691-13704.
[5] G. Licini, V. Conte, A. Coletti, M. Mba, C. Zonta, Coord. Chem. Rev. 255 (2011) 2345-2357.
[6] S. Ribeiro, A. Barbosa, A. Gomes, M. Pillinger, Fuel Process Technol. 116 (2013) 350-357.
[7] T. Ito, K. Inumaru, M. Misono, Chem. Mater. 13 (2001) 824-831.
[8] D. Long, E. Burkholder, L. Cronin, Chem. Soc. Rev. 36 (2007) 105-121.
[9] J. Toufaily, M. Soulard, L. Delmote, Colloids Surf A. 316 (2008) 285-291.
[10] D. Xie, Qihui He, Y. Su, T. Wang, R. Xu, B. Hu, Chin. J. Catal. 36 (2015) 1205-1213.
[11] J. Xiong, W. Zhu, W. Ding, L. Yang, M. Zhang, W. Jiang, Z. Zhao, RSC. Adv. 5 (2015) 16847-16855.
[12] J. Xiong, W. Zhu, H. Li, Y. Xu, W. Jiang, S. Xun, H. Liu, Z. Zhao, AIChE J. 59 (2013) 4696-4699.
[13] Sh. Tangestaninejad, M. Moghadam, V. Mirkhani, I. Mohammadpoor, E. Shams, H. Salavati, Ultrason. Sonochem. 15 (2008) 438-447.
[14] H. Salavati, N. Rasouli, Appl. Surf. Sci. 257 (2011) 4532-4538.
[15] H. Salavati, N. Rasouli, Mater. Res. Bull. 46 (2011) 1853-1859.
[16] Y. Chen, F. Zhang, Y. Fang, X. Zhu, Catal. Commun. 38 (2013) 54-58.
[17] H. Hamadi, M. Kooti, M. Afshari, Z. Ghiasifar, J. Mol. Catal. A 373 (2013) 25-29.
[18] X. Zheng, L.Zhang, J. Li, S. Luo, Chem. Commun. 47 (2011) 12325-12337.
[19] W.P. Wang, H. Yang, T. Xian, J.L. Jiang, Mater. Trans. 53 (2012) 1586-1589.
[20] Z. Zhang, F. Zhang, Q. Zhu, W. Zhao, J. Colloid Interface Sci. 360 (2011) 189-194.
[21] A. Pui, D. Gherca, G. Caria, Dig. J. Nanomater. Biostruct. 6 (2011) 1783-1791.
[22] M.I. Obaidat, B. Issa, Y.O. Haik, J. Nanomater. 5 (2015) 63-89.
[23] O. Veiseh, W. Jonathan, M. Zhang, Adv. Drug Delivery Rev. 62 (2010) 284-304.
[24] V. Haritha, H.M. Meshram, A.B. Rao, Green Sustain. Chem. 5 (2015) 25-30.
[25] S. Sobhani, Z. Pakdin-Parizi, J. Chem. Sci. 125 (2013) 975-979.
[26] S. German, M. Mamoun, Z. Andrei, Chem. Engin. Sci. 6 (2006) 4625-4633.
[27] G. Jianhua, Z. Yuming, Y. Yong, X. Mengwei, China Pet. Process. Petrochem. Technol. 14 (2012) 25-31.
[28] A. Ghosh, K. Sinha, P. Saha, Desalination Water Treat. 51 (2013) 7791-7799.
[29] J. Zhang, Y. Tang, G. Li, C. Hu, Appl. Catal A. 278 (2005) 251-261.
[30] M. Sertkol, Y. Koseoglu, A. Baykal, H. Kavas, A.C. Basaran, J. Magn. Magn. Mater. 321 (2009) 157-162.
[31] M.A. Rezvani, A.F. Shojaei, J. Serb. Chem. Soc. 79 (2014) 1099-1110.
[32] W. Trakarnpruk, K. Rujiraworawut, Fuel Process Technol. 90 (2009) 411-414.
[33] Y. Sasaki, K. Ushimaru, K. Iteya, H. Nakayama, S. Yamaguchi, Tetrahedron Lett. 45 (2004) 9513-9515.
[34] B. Karimi, M. Ghoreishinezhad, J.H. Clark, Org Lett. 7 (2005) 625-628.